Rapid Communications

Ideal intersecting nodal-ring phonons in bcc C_8

Y. J. Jin,[1] Z. J. Chen,[1,2] B. W. Xia,[1] Y. J. Zhao,[2] R. Wang,[1,3,*] and H. Xu[1,†]

[1]*Department of Physics and Institute for Quantum Science and Engineering, Southern University of Science and Technology, Shenzhen 518055, People's Republic of China*

[2]*Department of Physics, South China University of Technology, Guangzhou 510640, People's Republic of China*

[3]*Institute for Structure and Function and Department of Physics, Chongqing University, Chongqing 400044, People's Republic of China*

(Received 8 October 2018; published 21 December 2018)

Carbon, a basic versatile element in our universe, exhibits rich varieties of allotropic phases, most of which possess promising nontrivial topological fermions. In this work, we identify a distinct topological phonon phase in a realistic carbon allotrope with a body-centered cubic structure, termed bcc C_8. We show by symmetry arguments and effective model analysis that there are three intersecting phonon nodal rings perpendicular to each other in different planes. The intersecting phonon nodal rings are protected by time-reversal and inversion symmetries, which quantize the corresponding Berry phase into integer multiples of π. Unlike the electron systems, the phonon nodal rings in bcc C_8 are guaranteed to remain gapless due to the lack of spin-orbital coupling. The nearly flat drumhead surface states projected on semi-infinite (001) and (110) surfaces of bcc C_8 are clearly visible. Our findings not only discover promising nodal ring phonons in a carbon allotrope but also provide emergent avenues for exploring topological phonons beyond fermionic electrons in carbon-allotropic structures with attractive features.

DOI: 10.1103/PhysRevB.98.220103

Carbon is an extremely versatile element since it is able to form a vast number of allotropes with fascinating properties. Prominent members include graphite, diamond, carbon nanotubes [1], graphene [2], fullerenes, and other promising phases [3]. Among these allotropic phases, one of the most important members is graphene, a single atomic layer of carbon atoms in a honeycomb lattice. On the one hand, the discovery of graphene has triggered tremendous interest in two-dimensional (2D) materials [4–6]. On the other hand, more importantly, graphene significantly promotes advancements in studies of topological materials. As is well known, graphene possesses the unique electronic structure that exhibits topological semimetallic features with massless Dirac fermions in the absence of spin-orbital coupling (SOC) [7]. Furthermore, when the SOC effect is considered, the Dirac cone is destroyed and then graphene converts into a quantum spin Hall (QSH) insulator (i.e., 2D topological insulator) [8]. Topological insulators [9,10] and topological semimetals [11] have attracted extensive attention over the past decade. Beyond 2D graphene, nontrivial electronic states have also been intensively extended into three-dimensional (3D) carbon allotropes. For instance, the topological semimetallic phases have been predicted in 3D graphene networks [12–14], body-centered orthorhombic C_{16} [15], body-centered tetragonal C_{16} [16] and C_{40} [17], and beyond [18–23].

Overall, these advances provide exciting avenues for exploring band topology in carbon allotropes. Motivated by observations of topological fermions, we naturally raise a question: Are there carbon allotropes that can host topological bosons? In fact, besides nontrivial fermionic electrons, the topological states have recently been accessed into bosonic systems [24–34]. Within nontrivial bosons, topological phonons (i.e., quantized excited vibrational states of interacting atoms) are of particular importance, and provide potentially promising applications of electron-phonon coupling, dynamic instability [35], and phonon diode [36]. Very recently, topological phonons at THz frequencies have been proposed in a few materials, such as double Weyl phonons in transition-metal monosilicides [31,32], Weyl and triple phonons in WC-type compounds [33], and Weyl nodal straight line phonons in MgB_2 [34]. However, realistic candidates with topological phonons discovered to date are very limited. As the topological orders in carbon allotropic materials host the most attractive features, it is highly desirable to explore topological phonon states in carbon allotropes.

In this work, using first-principles calculations and topological analysis, we identify a carbon allotrope with a body-centered cubic (bcc) structure in space group $Im\text{-}3m$ (no. 229) that exhibits exotic topological phonon states. This carbon phase contains eight atoms in one primitive unit cell, thus termed bcc C_8. We show by symmetry arguments that bcc C_8 hosts three phonon nodal rings in different planes intersecting at six different points. We reveal the quantized Berry phase and drumhead surface states to further support its topological phonon features. Importantly, bcc C_8 has already been synthesized in experiments [37,38], suggesting that it is of fundamental importance and practical interest to establish a realistic carbon phase with intriguing nontrivial phonons.

We performed first-principles calculations based on density functional theory [39] as implemented in the Vienna *ab initio* simulation package [40]. The generalized gradient

*rcwang@cqu.edu.cn
†xuh@sustc.edu.cn

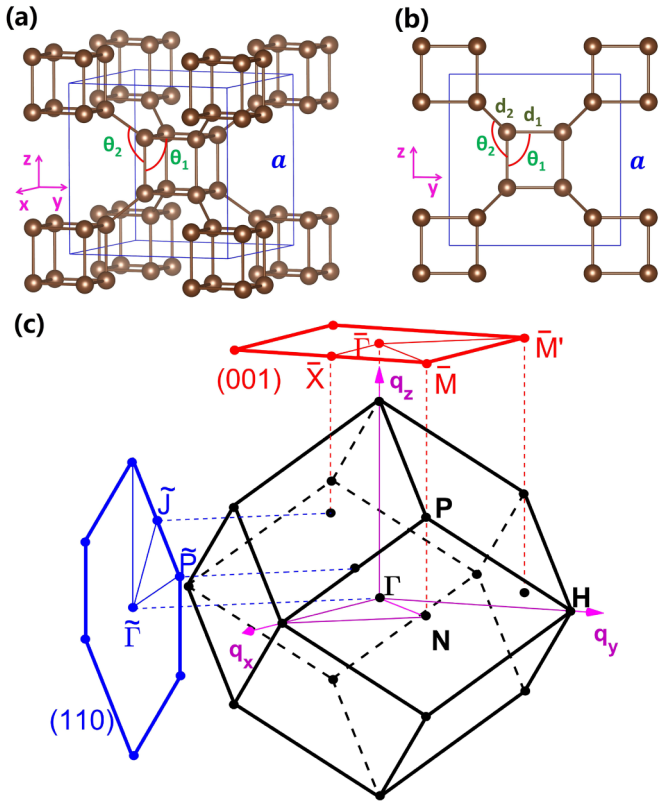

FIG. 1. (a) Side and (b) top views of bcc C_8 crystallized in space group *Im-3m* (no. 229). The two distinct bond lengths (d_1, d_2) and bond angles (θ_1, θ_2) are denoted. (c) The bulk BZ and its corresponding surface BZ projected on the (001) and (110) surfaces, respectively.

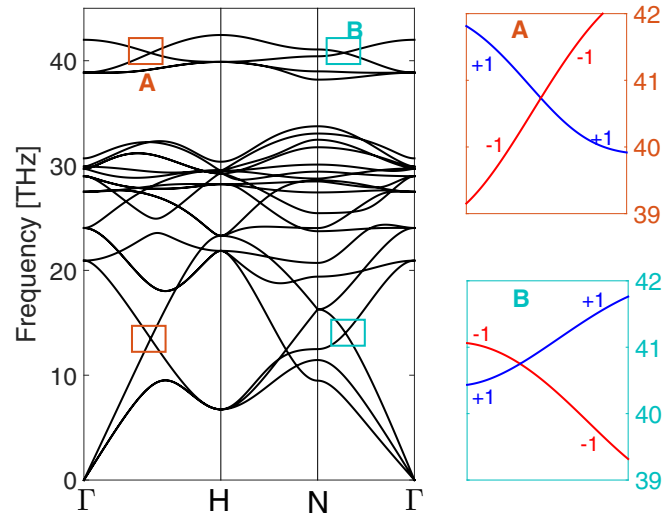

FIG. 2. The phonon spectra of bcc C_8 along high-symmetry lines. The right panels show the enlarged regions A and B, respectively. Two crossing branches in the Γ-*H* and Γ-*N* directions are classified by opposite mirror eigenvalues ±1.

approximation with Perdew-Burke-Ernzerhof functional was employed to describe exchange-correlation energy. The core-valence interactions were treated by the projector augmented wave method [41,42]. The cutoff energy of plane wave was taken as 500 eV, and the Brillouin zone (BZ) was sampled by $12 \times 12 \times 12$ Monkhorst-Pack grid [43]. The structural parameters of bcc C_8 were optimized by minimizing the forces on each atom smaller than 1.0×10^{-3} eV/Å. We calculated lattice dynamics using density-functional perturbation theory (DFPT) [44] with a $3 \times 3 \times 3$ supercell. The phonon spectra were obtained by diagonalization of real-space force constants as implemented in the PHONOPY package [45]. In order to reveal nontrivial features of phonons in bcc C_8, we also constructed a Wannier tight-binding (TB) Hamiltonian of phonons from the second rank tensor of force constants [45].

As shown in Figs. 1(a) and 1(b), we can see that each lattice point in bcc C_8 consists of eight carbon atoms forming a subcube, and each carbon atom bonds to four neighbors showing a distorted tetrahedron. The eight carbon atoms in one primitive unit cell occupy an equivalent Wyckoff position of 16f (−0.3374, −0.3374, 0.3374). Its optimized lattice constant is $a = 4.87$ Å, which is in good agreement with the experimental value [37]. In contrast to the unique bond length in 2D graphene or 3D diamond, there are two distinct carbon-carbon bond lengths. The longer bond $d_1 = 1.586$ Å is associated with intrabonds in a subcube, and the shorter one $d_2 = 1.476$ Å connects two neighboring subcubes. There are also two different bond angles, i.e., $\theta_1 = 90^\circ$ in a subcube and $\theta_2 = 125.26^\circ$ out of a subcube. In Fig. 1(c), we show the bulk BZ and the (001) and (110) surface BZs, in which high-symmetry points are marked.

The phonon spectra of bcc C_8 along the high-symmetry paths of the BZ are plotted in the left panel of Fig. 2. It is clear to see that there are two sets of visible double-degenerate points in both the Γ-*H* and Γ-*N* directions. One comes from the crossing of the longitudinal acoustic branch and the lowest transverse optical branch, and the other is originated from the crossing of two highest optical branches. As phonons are typically bosons, they are not limited by the Pauli exclusion principle. That is to say, the topological features in the whole range of phonon frequencies can be detected. Besides, there are also many other crossing points below the frequency of 30 THz. They do not form any nodal rings but result in plenty of discrete degenerate points, including trivial and nontrivial ones. Because of overlap of bulk phonon branches, the phonon surface states in this frequency region are hidden in the projected bulk states and invisible. Therefore, we here only focus on the crossings of two highest optical branches, for which the two nontrivial crossing branches are well separated from trivial ones. As shown in the right panels of Fig. 2, the enlarged views of phonon spectra show the crossing points in the Γ-*H* and Γ-*N* directions at the same frequency of $\omega_D = 40.75$ THz. Actually, these crossings with linear dispersions are in the q_x-q_y plane with $q_z = 0$, which is with respect to the mirror reflection symmetry M_z. The two crossing branches within this mirror-reflection invariant plane belong to two opposite mirror eigenvalues ±1. A 3D plot of these crossing branches with $q_z = 0$ is present in Fig. 3(a). The figure shows that the crossings of two inverted branches form a continuous phonon nodal ring. The nodal ring exhibits no frequency dispersion in the q_x-q_y plane. This ideal feature of topological phonons in bcc C_8 can be easily detected and is important

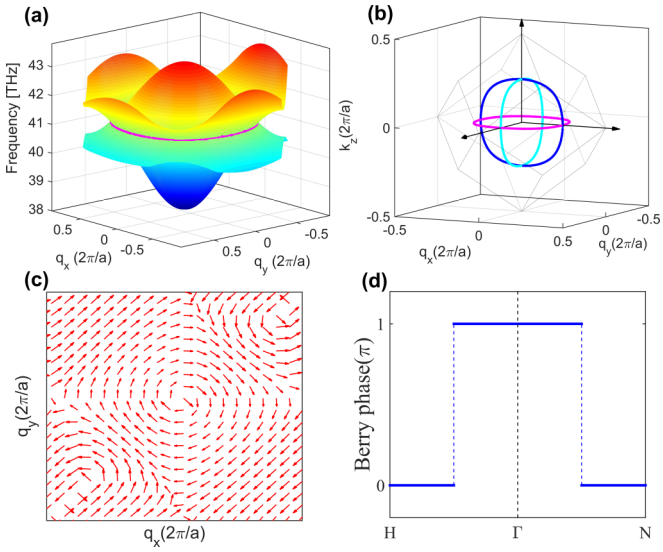

FIG. 3. (a) Two crossing branches optical phonons forming a nodal ring (colored by pink) in the q_x-q_y plane with $q_z = 0$. (b) Three intersecting phonon nodal rings (colored by pink, blue, and light blue, respectively) in three different planes in 3D momentum space. (c) Berry curvature distribution of a nodal ring in the q_x-q_y plane with $k_z = 0$. (d) A variation of Berry phase along the high-symmetry paths H-Γ-N in the q_x-q_y plane with $q_z = 0$.

to applications of topological quantum transport of phonons. Besides the phonon nodal ring in the q_x-q_y plane, we also find another two phonon nodal rings in the q_x-q_z plane and q_y-q_z plane, respectively. As depicted in Fig. 3(b), the three phonon nodal rings perpendicular to each other in different planes intersect at six points.

Next, we prove the existence of three intersecting phonon nodal rings encircling the Γ point by an effective $\mathbf{k}\cdot\mathbf{p}$ model. The symmetry at the Γ point of bcc C_8 is characterized by O_h, which includes inversion symmetry $\mathcal{I}$, four-fold rotational symmetries C_4 around the x, y, and z axes, and mirror-reflection symmetries M_x, M_y, and M_z. In general, the two crossing branches of phonons can be described by a 2×2 low-energy $\mathbf{k}\cdot\mathbf{p}$ Hamiltonian as

$$\mathcal{H}(\mathbf{q}) = \sum_{i=x,y,z} d_i(\mathbf{q})\sigma_i, \tag{1}$$

where $\mathcal{H}$ is referenced to the frequency of a crossing point, $d_i(\mathbf{q})$ are real functions, $\mathbf{q} = (q_x, q_y, q_z)$ is the phonon wave vector, and σ_i are three Pauli matrices. The identity matrix σ_0 only shifts degenerate points of phonons and can be ignored in Eq. (1) in the following. The two crossing branches of phonons around the Γ point have the opposite eigenvalues, indicating that the $\mathcal{I}$ symmetry can be chosen as $\mathcal{I} = \sigma_z$. The Hamiltonian has the following constraint as

$$\mathcal{I}\mathcal{H}(\mathbf{q})\mathcal{I}^{-1} = \mathcal{H}(-\mathbf{q}), \tag{2}$$

which means that $d_{x,y}(\mathbf{q})$ are odd functions and $d_z(\mathbf{q})$ is an even function. Besides, phonons are typically spinless [46], and thus the time-reversal ($\mathcal{T}$) symmetry of a phonon system is always conserved when there is no any strain-gradient field. The absence of SOC indicates $\mathcal{T}^2 = 1$; that is, the $\mathcal{T}$ symmetry can be represented by $\mathcal{T} = K$, where K is the complex conjugate operator. The $\mathcal{T}$ symmetry requires

$$\mathcal{T}\mathcal{H}(\mathbf{q})\mathcal{T}^{-1} = \mathcal{H}(-\mathbf{q}), \tag{3}$$

which gives a constraint leading to $d_{x,z}(\mathbf{q})$ being even functions and $d_y(\mathbf{q})$ being an odd function. As a result, the coexistence of $\mathcal{I}$ and $\mathcal{T}$ symmetries gives $d_x(\mathbf{q}) \equiv 0$, $d_y(\mathbf{q}) = -d_y(-\mathbf{q})$, and $d_z(\mathbf{q}) = d_z(-\mathbf{q})$. The symmetry-allowed expressions as a function of $\mathbf{q}$ in the low energy can be generally written as

$$\begin{aligned} d_y(\mathbf{q}) &= \sum_{i=x,y,z} C^i_{1y} q_i + \sum_{i,j,k=x,y,z} C^{ijk}_{3y} q_i q_j q_k, \\ d_z(\mathbf{q}) &= C_{0z} + \sum_{i,j=x,y,z} C^{ij}_{2z} q_i q_j. \end{aligned} \tag{4}$$

The generic solutions of two phonon crossing branches require $d_y(\mathbf{q}) = 0$ and $d_z(\mathbf{q}) = 0$. Based on Eq. (4), this condition has codimension 1, allowing nodal lines in momentum space. The rotational symmetries C^i_4 ($i = x, y, z$) and mirror symmetries M_i introduce additional symmetry constraints on $d_y(\mathbf{q})$ and $d_z(\mathbf{q})$. Under these symmetries, Eq. (4) can be reduced as

$$\begin{aligned} d_y(\mathbf{q}) &= C^{xyz}_{3y} q_x q_y q_z, \\ d_z(\mathbf{q}) &= C_{0z} + C^{xx}_{2z}\left(q_x^2 + q_y^2 + q_z^2\right), \end{aligned} \tag{5}$$

where the condition of band inversion requires $C_{0z}C^{xx}_{2z} < 0$. In this case, Eq. (5) indicates the appearance of three intersecting closed nodal rings perpendicular to each other in the q_x, q_y, and $q_z = 0$ planes. These planes are mirror-reflection invariant. However, it is worth noting that the stability of phonon nodal rings in bcc C_8 is topologically protected by the coexistence of $\mathcal{I}$ and $\mathcal{T}$ symmetries. The additional rotational and mirror symmetries just force the phonon nodal rings to be related to C_4 symmetries around the q_x, q_y, and q_y axes and lie in the q_x, q_y and $q_z = 0$ planes, respectively. Because of the lack of the SOC effect in a phonon system, the phonon nodal rings in bcc C_8 are generally robust and guaranteed to be gapless with respect to perturbations as long as $\mathcal{I}$ and $\mathcal{T}$ symmetries are present.

The presence of topological phonon nodal rings corresponds to Berry phase quantization [47]. The Berry phase of a closed loop $\mathcal{C}$ in 3D momentum space is defined as

$$\gamma = \oint_{\mathcal{C}} \mathcal{A}(\mathbf{q})\cdot d\mathbf{q}, \tag{6}$$

where $\mathcal{A}(\mathbf{q}) = -i\sum_\lambda \langle\varphi_\lambda(\mathbf{q})|\nabla_{\mathbf{q}}|\varphi_\lambda(\mathbf{q})\rangle$ is the Berry connection and $\varphi_\lambda(\mathbf{q})$ is the Bloch wave function of the λth phonon branch. The phonon Bloch wave function can be written as [36]

$$\varphi_\lambda(\mathbf{q}) = \begin{pmatrix} \mathcal{D}^{1/2}_{\mathbf{q}}\mathbf{u}_{\mathbf{q}} \\ \dot{\mathbf{u}}_{\mathbf{q}} \end{pmatrix}, \tag{7}$$

where $\mathcal{D}(\mathbf{q})$ is the lattice dynamic matrix, $\mathbf{u}_{\mathbf{q}}$ represents the atomic eigen displacement, and $\dot{\mathbf{u}}_{\mathbf{q}}$ is its time derivative. Equation (7) indicates that we are able to calculate the phonon Berry connection $\mathcal{A}(\mathbf{q})$ using atomic force constants, which can conveniently be obtained from DFPT [44]. The corresponding phonon Berry curvature is $\mathcal{B}(\mathbf{q}) = \nabla\times\mathcal{A}(\mathbf{q})$. As shown in Fig. 3(c), the distribution of Berry curvature in the

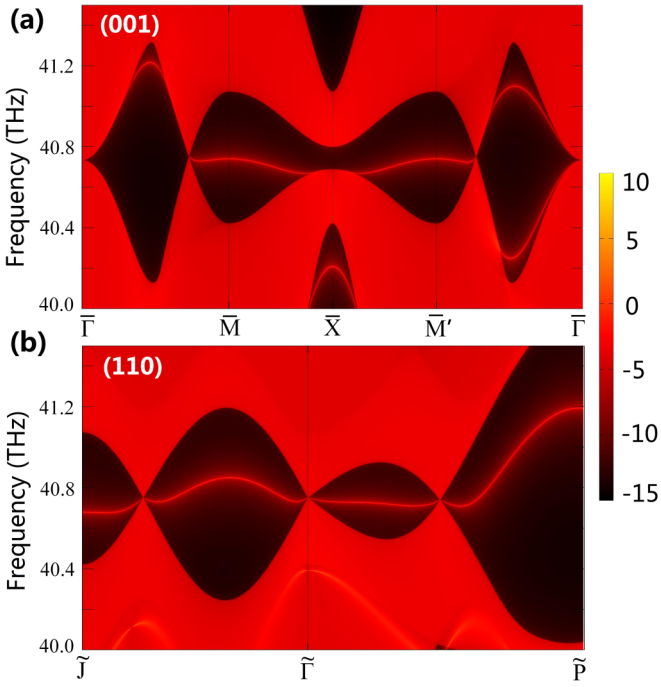

FIG. 4. The phonon surface states of bcc C_8. (a) LDOS projected on the semi-infinite (001) surface. (b) LDOS projected on the semi-infinite (110) surface. Both the surfaces are terminated at the subcube. Red regions represent the projections of bulk phonon branches, and red lines represent the phonon surface states. The nontrivial drumhead surface states terminated at the projections of phonon crossing points are nearly flat and clearly visible.

$q_z = 0$ plane exhibits a nontrivial vortex feature in momentum space. To further support the topologically protected phonon nodal rings, we also calculate a variation of phonon Berry phase in the $q_z = 0$ plane, which corresponds to the one-dimensional system along the high-symmetry paths H-Γ-N. Figure 3(d) shows a jump of π across the nodal ring, confirming the nontrivial phonon Berry phase (π mod 2π) of the phonon nodal ring in bcc C_8.

The topological phonon nodal rings with quantized Berry phase lead to the nontrivial drumhead surface states. To directly illustrate this, we calculate the local density of states (LDOS) of phonons with the iterative Green's function method based on a phonon TB Hamiltonian [48,49]. In Figs. 4(a) and 4(b), we plot the LDOS projected on the semi-infinite (001) and (110) surfaces of bcc C_8 terminated at the subcube, respectively. As expected, the topological drumhead surface states terminated at the projections of phonon crossing points are nearly flat and clearly visible. On the (001) surface, the bulk Dirac cones along $\bar{\Gamma}$-$\bar{M}$ and $\bar{\Gamma}$-$\bar{M}'$ are projected from the nodal ring in the $q_z = 0$ plane. As the appearance of surface breaks the C_4 rotational symmetry, the surface states along $\bar{\Gamma}$-$\bar{M}$ and $\bar{\Gamma}$-$\bar{M}'$ in the square (001) surface BZ are nonequivalent [see Fig. 4(a)]. On the (110) surface, the bulk Dirac cone at the $\tilde{\Gamma}$ point is projected from two overlapping crossing points on the $q_x = -q_y$ axis across the nodal ring in the plane of $q_z = 0$, while the bulk Dirac cone along $\tilde{\Gamma}$-$\tilde{J}$ (or $\tilde{\Gamma}$-$\tilde{P}$) is projected from crossing points of two superimposed nodal rings lied in the planes of $q_x = 0$ and $q_y = 0$. As a result, the intersecting orthogonal nodal rings in bcc C_8 derive that the bulk Dirac cones projected on the (110) surface are connected by two nontrivial surface states.

In summary, using first-principles and effective model analysis, we propose an emergent topological bosonic phase in which nontrivial phonons are present in a carbon allotrope bcc C_8. In this exotic topological phase, there are three intersecting phonon nodal rings perpendicular to each other in different planes. The symmetry arguments indicate that these intersecting phonon nodal rings are protected by time-reversal and inversion symmetries. Because of the lack of SOC in phonon systems, the phonon nodal rings in bcc C_8 are generally guaranteed to remain intact with respect to perturbations. Our calculations confirm that the Berry phase is quantized into integer multiples of π. The nearly flat drumhead surface states projected on the semi-infinite (001) and (110) surfaces of bcc C_8 are clearly visible, further supporting the topological phonon features. Our findings not only provide exciting avenues for exploring topological phonons beyond nontrivial fermions in carbon allotropic structures but also establish a realistic carbon allotrope with intriguing nontrivial phonons.

This work is supported by the National Natural Science Foundation of China (NSFC, Grants No. 11674148 and No. 11304403), the Guangdong Natural Science Funds for Distinguished Young Scholars (Grant No. 2017B030306008), and the Fundamental Research Funds for the Central Universities of China (Grants No. 106112017CDJXY300005 and No. cqu2018CDHB1B01).

[1] S. Iijima, Nature (London) **354**, 56 (1991).
[2] A. H. Castro Neto, F. Guinea, N. M. R. Peres, K. S. Novoselov, and A. K. Geim, Rev. Mod. Phys. **81**, 109 (2009).
[3] H. Niu, X.-Q. Chen, S. Wang, D. Li, W. L. Mao, and Y. Li, Phys. Rev. Lett. **108**, 135501 (2012).
[4] K. F. Mak, C. Lee, J. Hone, J. Shan, and T. F. Heinz, Phys. Rev. Lett. **105**, 136805 (2010).
[5] P. Vogt, P. De Padova, C. Quaresima, J. Avila, E. Frantzeskakis, M. C. Asensio, A. Resta, B. Ealet, and G. Le Lay, Phys. Rev. Lett. **108**, 155501 (2012).
[6] S. Manzeli, D. Ovchinnikov, D. Pasquier, O. V. Yazyev, and A. Kis, Nat. Rev. Mater. **2**, 17033 (2017).
[7] D. Xiao, W. Yao, and Q. Niu, Phys. Rev. Lett. **99**, 236809 (2007).
[8] C. L. Kane and E. J. Mele, Phys. Rev. Lett. **95**, 226801 (2005).
[9] M. Z. Hasan and C. L. Kane, Rev. Mod. Phys. **82**, 3045 (2010).
[10] X.-L. Qi and S.-C. Zhang, Rev. Mod. Phys. **83**, 1057 (2011).
[11] N. P. Armitage, E. J. Mele, and A. Vishwanath, Rev. Mod. Phys. **90**, 015001 (2018).
[12] H. Weng, Y. Liang, Q. Xu, R. Yu, Z. Fang, X. Dai, and Y. Kawazoe, Phys. Rev. B **92**, 045108 (2015).
[13] Y. Chen, Y. Xie, S. A. Yang, H. Pan, F. Zhang, M. L. Cohen, and S. Zhang, Nano Lett. **15**, 6974 (2015).

[14] J.-T. Wang, C. Chen, and Y. Kawazoe, Phys. Rev. B **97**, 245147 (2018).
[15] J.-T. Wang, H. Weng, S. Nie, Z. Fang, Y. Kawazoe, and C. Chen, Phys. Rev. Lett. **116**, 195501 (2016).
[16] Y. Cheng, X. Feng, X. Cao, B. Wen, Q. Wang, Y. Kawazoe, and P. Jena, Small **13**, 1602894 (2017).
[17] J.-T. Wang, S. Nie, H. Weng, Y. Kawazoe, and C. Chen, Phys. Rev. Lett. **120**, 026402 (2018).
[18] X. Dong, M. Hu, J. He, Y. Tian, and H.-T. Wang, Sci. Rep. **5**, 10713 (2015).
[19] X. Feng, Q. Wu, Y. Cheng, B. Wen, Q. Wang, Y. Kawazoe, and P. Jena, Carbon **127**, 527 (2018).
[20] C. Zhong, Y. Chen, Z.-M. Yu, Y. Xie, H. Wang, S. A. Yang, and S. Zhang, Nat. Commun. **8**, 15641 (2017).
[21] Y. Cheng, J. Du, R. Melnik, Y. Kawazoe, and B. Wen, Carbon **98**, 468 (2016).
[22] C. Zhong, Y. Chen, Y. Xie, S. A. Yang, M. L. Cohen, and S. B. Zhang, Nanoscale **8**, 7232 (2016).
[23] K. Mullen, B. Uchoa, and D. T. Glatzhofer, Phys. Rev. Lett. **115**, 026403 (2015).
[24] F. D. M. Haldane and S. Raghu, Phys. Rev. Lett. **100**, 013904 (2008).
[25] Z. Wang, Y. D. Chong, J. D. Joannopoulos, and M. Soljačić, Phys. Rev. Lett. **100**, 013905 (2008).
[26] S. H. Mousavi, A. B. Khanikaev, and Z. Wang, Nat. Commun. **6**, 8682 (2015).
[27] C. He, X. Ni, H. Ge, X.-C. Sun, Y.-B. Chen, M.-H. Lu, X.-P. Liu, and Y.-F. Chen, Nat. Phys. **12**, 1124 (2016).
[28] R. Süsstrunk and S. D. Huber, Science **349**, 47 (2015).
[29] F. Li, X. Huang, J. Lu, J. Ma, and Z. Liu, Nat. Phys. **14**, 30 (2018).
[30] F. Liu, H.-Y. Deng, and K. Wakabayashi, Phys. Rev. B **97**, 035442 (2018).
[31] T. Zhang, Z. Song, A. Alexandradinata, H. Weng, C. Fang, L. Lu, and Z. Fang, Phys. Rev. Lett. **120**, 016401 (2018).
[32] H. Miao, T. T. Zhang, L. Wang, D. Meyers, A. H. Said, Y. L. Wang, Y. G. Shi, H. M. Weng, Z. Fang, and M. P. M. Dean, Phys. Rev. Lett. **121**, 035302 (2018).
[33] J. Li, Q. Xie, S. Ullah, R. Li, H. Ma, D. Li, Y. Li, and X.-Q. Chen, Phys. Rev. B **97**, 054305 (2018).
[34] Q. Xie, J. Li, M. Liu, L. Wang, D. Li, Y. Li, and X.-Q. Chen, arXiv:1801.04048 (unpublished).
[35] E. Prodan and C. Prodan, Phys. Rev. Lett. **103**, 248101 (2009).
[36] Y. Liu, Y. Xu, S.-C. Zhang, and W. Duan, Phys. Rev. B **96**, 064106 (2017).
[37] N. N. Matyushenko, V. E. Strel'nitskii, and V. A. Gusev, Pis'ma Zh. Eksp. Teor. Fiz. **30**, 218 (1979) [JETP Lett. **30**, 199 (1979)].
[38] R. L. Johnston, and R. Hoffmann, J. Am. Chem. Soc. **111**, 810 (1989).
[39] W. Kohn and L. J. Sham, Phys. Rev. **140**, A1133 (1965).
[40] G. Kresse and J. Furthmüller, Phys. Rev. B **54**, 11169 (1996).
[41] G. Kresse and D. Joubert, Phys. Rev. B **59**, 1758 (1999).
[42] D. M. Ceperley and B. J. Alder, Phys. Rev. Lett. **45**, 566 (1980).
[43] H. J. Monkhorst and J. D. Pack, Phys. Rev. B **13**, 5188 (1976).
[44] S. Baroni, S. de Gironcoli, A. Dal Corso, and P. Giannozzi, Rev. Mod. Phys. **73**, 515 (2001).
[45] A. Togo and I. Tanaka, Scr. Mater. **108**, 1 (2015).
[46] A. T. Levine, Nuovo Cimento **26**, 190 (1962).
[47] C. Fang, Y. Chen, H.-Y. Kee, and L. Fu, Phys. Rev. B **92**, 081201(R) (2015).
[48] M. P. L. Sancho, J. M. L. Sancho, and J. Rubio, J. Phys. F **14**, 1205 (1984).
[49] Q. Wu, S. Zhang, H.-F. Song, M. Troyer, and A. A. Soluyanov, Comput. Phys. Commun. **224**, 405 (2018).